Time-Dependent Density Functional Theory for X-Ray Absorption Spectra: Comparing the Real-Time Approach to Linear Response

John M. Herbert,[1,2*] Ying Zhu,[1,2] Bushra Alam,[1] and Avik Kumar Ojha[1]
[1] *Department of Chemistry & Biochemistry, The Ohio State University, Columbus, Ohio, 43210 USA and*
[2] *Chemical Physics Graduate Program, The Ohio State University, Columbus, Ohio, 43210 USA*
(Dated: June 18, 2023)

Abstract

We examine the simulation of x-ray absorption spectra at elemental K-edges using time-dependent density functional theory, in both its conventional linear-response implementation and also its "real-time" formulation. Real-time simulations enable broadband x-ray spectra calculations without the need to invoke frozen occupied orbitals or "core/valence separation", but we find that the spectra are frequently contaminated by transitions to the continuum originating from lower-energy core and semi-core orbitals. This problem becomes acute in triple-ζ basis sets although it is sometimes bypassed serendipitously in lower-quality basis sets. Transitions to the continuum acquire surprisingly large dipole oscillator strengths, leading to spectra that are difficult or impossible to interpret. Meaningful spectra can be recovered by means of a filtering technique that decomposes the spectrum into contributions from individual occupied orbitals, and the same procedure can be used to separate L- and K-edge spectra. Nevertheless, the conventional linear-response approach is significantly more efficient even when hundreds of individual states are needed to reproduce near-edge absorption features, and even when Padé approximants are used to reduce the real-time simulations to less than 2 fs of time propagation. The real-time approach may be useful for examining the validity of core/valence separation, however.

1 Introduction

Quantum chemistry is currently witnessing a surge of interest in x-ray spectroscopy,[1–9] catalyzed by the emergence of new technologies including coherent ultrahigh harmonic generation[10] that provide capabilities for ultrafast time resolution at x-ray wavelengths,[11–13] even with tabletop laser systems.[14] This technology has enabled x-ray absorption spectroscopy (XAS) and x-ray photoelectron spectroscopy (XPS) studies of solution-phase systems,[15–18] as well as surface-sensitive ultrafast spectroscopy at extreme ultraviolet (XUV) wavelengths.[19] Insofar as XAS is a widely-used tool to interrogate bonding and oxidation state, these advances offer the possibility to study element-specific charge dynamics with ultrafast time resolution, and electronic structure theory will undoubtedly play a major role in interpreting the results.

Although there are several methods to obtain excited states in density functional theory (DFT),[20] the most widely used is the linear-response (LR) formulation of time-dependent DFT,[20–25] which we call LR-TDDFT here but which is so ubiquitous in modern quantum chemistry that it is usually just called "TDDFT". Its computational cost and storage requirements scale as $\mathcal{O}(no^2v^2)$ and $\mathcal{O}(nov)$,[20] respectively, where o and v are the number of occupied and virtual orbitals and n is the number of excited states. That number is prohibitively large for core-level excitations unless an active-space approximation is invoked,[26] including only a few core orbitals along with the full virtual space, such that core-to-valence excitations appear as the lowest-energy states in the spectrum. (In principle, interior eigensolvers could be used for core-level excitations[27–29] but that approach has not been widely used.) In many-body theory, this active-space approximation is known as "core/valence separation" (CVS),[1,30–34] whereas in LR-TDDFT it has also been called a "restricted excitation window",[5,35] and it amounts to freezing most of the occupied orbitals. For K-edge transitions (*i.e.*, those originating from 1s orbitals in the occupied space), this approximation introduces errors of ± 0.02 eV provided that high-quality basis sets are used,[36] although larger errors have been suggested in complete active space self-consistent field calculations.[29] It is less clear what the errors might be for L- or M-edge excitations that originate from orbitals with higher principle quantum number, which may not be energetically separated from other valence orbitals. Furthermore, hundreds of states may be required to compute near-edge x-ray adsorption fine structure (NEXAFS) spectra.

In the present work, we consider an alternative formulation of TDDFT in which broadband spectra are simulated via solution of the time-dependent Kohn-Sham (TDKS) equation,[37–41] in what is sometimes called "real-time" TDDFT.[20,42,43] This is potentially attractive for XAS because the requisite computational resources are independent of the number of excited states. Instead, the spectrum is obtained via Fourier transform of the dipole autocorrelation function following sufficient time propagation of complex-valued molecular orbitals (MOs). The total memory requirement scales as $\mathcal{O}(o^2)$, as in ground-state DFT. The computational resources do depend on the energy regime of interest, as a smaller integration

*herbert@chemistry.ohio-state.edu

time step (Δt) is required to reach higher excitation energies because these correspond to higher-frequency Fourier components of the signal. That said, for large systems the finite-Δt error may be more easily controllable as compared to errors engendered by truncation of the excitation space in LR-TDDFT, because the former can be reduced with smaller time steps and longer propagation times whereas enlarging the excitation space may encounter hardware (storage) limitations.

The TDKS and LR-TDDFT approaches are formally[20–23,39] and operationally[44,45] equivalent in the limit of a weak perturbation to the ground state, provided that the full basis of $o \times v$ excitation vectors is employed in the LR-TDDFT approach. As such, TDKS calculations reveal the true TDDFT spectrum in the absence of any truncations. This might be important in characterizing how the CVS approximation impacts L- and M-edge spectra and for this reason we investigate TDKS calculations of XAS in the present work, beginning (for simplicity) with elemental K-edge spectra. In so doing, we discovered that a recently reported "intruder state" problem[46] appears to be ubiquitous and pervasive in high-quality basis sets. This issue renders the TDKS approach unusable except in a modified form that is described herein.

2 Theory

This section provides a self-contained description of the TDKS method (Section 2 A), which is not yet widespread for excited-state calculations in molecules. The more common LR-TDDFT approach is introduced briefly in Section 2 B.

2.A. TDKS approach. A rigorous description of TDKS theory from first principles can be found in Refs. 38–40, whereas the present discussion is focused on practical considerations for computing absorption spectra. The adiabatic approximation[20,39] (*i.e.*, locality in time) is made throughout, so that the time dependence of the exchange-correlation functional is carried strictly by the time-evolving density, $\rho(\mathbf{r}, t)$. As such, ground-state exchange-correlation functionals are used without alteration.

2.A.1. Time propagation. The time-dependent density $\rho(\mathbf{r}, t)$ is represented in terms of time-dependent MOs,

$$\rho(\mathbf{r}, t) = \sum_{k}^{\text{occ}} |\psi_k(\mathbf{r}, t)|^2 \, . \tag{1}$$

Following a perturbation to the ground-state density at $t = 0$, the MOs $\psi_k(\mathbf{r}, t)$ propagate in time according to the equation

$$\mathrm{i}\hbar \frac{d\psi_k}{dt} = \hat{F}\psi_k(\mathbf{r}, t) \, , \tag{2}$$

which is a one-electron analogue of the time-dependent Schrödinger equation. Here, $\hat{F}$ is the effective one-electron Hamiltonian (Fock operator). The TDKS equations are numerically integrated in time to obtain $\{\psi_k(\mathbf{r}, t)\}$ from the ground-state MOs $\{\psi_k(\mathbf{r}, 0)\}$, the latter of which are eigenfunctions of $\hat{F}$:

$$\hat{F}\psi_k(\mathbf{r}, 0) = \varepsilon_k \psi_k(\mathbf{r}, 0) \, . \tag{3}$$

A perturbative solution of Eq. (2) affords the LR-TDDFT equations.[23]

The TDKS equation [Eq. (2)] is equivalent to the Liouville-von Neumann equation,

$$\mathrm{i}\hbar \frac{\partial \mathbf{P}}{\partial t} = \mathbf{FP} - \mathbf{PF}^\dagger \, . \tag{4}$$

Here, $\mathbf{P}(t)$ is the matrix representation of $\rho(\mathbf{r}, t)$ in an orthonormal basis, such as the initial ground-state MOs established by Eq. (3) or the time-evolved orbitals $\{\psi_k(\mathbf{r}, t)\}$. Integration of Eq. (4) affords

$$\mathbf{P}(t + \Delta t) = \mathbf{U}(t + \Delta t, t) \, \mathbf{P}(t) \, \mathbf{U}^\dagger(t + \Delta t, t) \tag{5}$$

where $\mathbf{U}(t + \Delta t)$ is a unitary time evolution operator for the time step $t \to t + \Delta t$. Because both $\mathbf{P}(t)$ and $\mathbf{F}(t)$ in Eq. (4) are time-dependent quantities, the definition of $\mathbf{U}(t + \Delta t)$ involves time-ordering of $\mathbf{F}(t')$ at points t' along the integration ($t \leq t' \leq t + \Delta t$), or else a Magnus expansion of nested commutators.[45] Various forms for $\mathbf{U}(t + \Delta t)$ have been discussed in the literature,[45,47–52] including adaptive schemes[52] and methods that iterate to self-consistency over the course of a time step from t to $t + \Delta t$.[45]

Because the energy scales for x-ray excitation are large, the corresponding time step needs to be small. For that reason, we use the modified-midpoint algorithm,[48] which is computationally simple (one Fock build per time step) and stable when Δt is small. The time step also determines the highest frequency-domain Fourier component that can described by the finite time series of dipole moment data that provide the absorption spectrum (see Section 2 A 2). Specifically, the Nyquist sampling theorem[53] limits the signal to frequencies $\omega \leq \omega_{\text{max}}$ where

$$\omega_{\text{max}} = \pi / \Delta t \, , \tag{6}$$

although we have previously found that well-converged spectra require somewhat smaller time steps,[45] or in other words the spectrum should be considered to be converged only if $E \ll \hbar\omega_{\text{max}}$.

2.A.2. Absorption spectra. The absorption cross section $S(\omega)$ from a TDKS calculation is computed from the

imaginary part of the trace of the frequency-dependent polarizability tensor,

$$S(\omega) = \left(\frac{4\pi\omega}{3c}\right) \mathfrak{Im}\big[\alpha_{xx}(\omega) + \alpha_{yy}(\omega) + \alpha_{zz}(\omega)\big] \quad (7)$$

where

$$\alpha_{\lambda\kappa}(\omega) = \frac{\partial \mu_\lambda(\omega)}{\partial \mathcal{E}_\kappa(\omega)} \quad (8)$$

for $\lambda, \kappa \in \{x, y, z\}$. The quantity $\alpha_{\lambda\kappa}(\omega)$ describes the frequency-domain response of the dipole moment (in direction λ) to an applied electric field $\mathcal{E}_\kappa(\omega)$ in direction κ.

In practice, the spectrum is obtained (up to an overall constant) as $S(\omega) = \sum_\lambda |d_\lambda(\omega)|^2$, where

$$d_\lambda(\omega) \propto \omega^2 \mu_\lambda(\omega) \quad (9)$$

is the dipole acceleration function.[54,55] The requisite frequency-dependent dipole moment function can be calculated via discrete Fourier transform of the time-dependent dipole moment,

$$\mu_\lambda(\omega) = \sum_{k=0}^{M} \mu_\lambda(t_k)\, e^{-\mathrm{i}\omega t_k} \ . \quad (10)$$

Here, M is the total number of time steps and $t_k = k\Delta t$. In a TDKS calculation, one computes the time dependent density $\rho(\mathbf{r}, t)$ by solving either Eq. (2) or Eq. (4), from which one can calculate $\mu_\lambda(t)$, leading ultimately to an absorption spectrum. The frequency resolution of that absorption spectrum improves as the total simulation time ($t_{\max} = M\Delta t$) is increased.

Integration time steps on the order of $\Delta t = 0.02$–0.20 a.u. are common,[44,45,56–60] where the atomic unit of time is ≈ 0.0242 fs. Values on the smaller end of that range are necessary for XAS, due to the Fourier transform limit on the maximum excitation energy, Eq. (6). A total propagation time $t_{\max} = 10$–30 fs is typically required in order to obtain an adequately converged spectrum,[44,45,56–59] which equates to 10,000 or more time steps. The cost of each step is roughly equivalent to that of one self-consistent field (SCF) iteration of a ground-state DFT calculation, when the modified-midpoint algorithm is used.[48]

2.A.3. Padé-accelerated transforms. The requisite propagation time can be reduced through the application of a Padé-accelerated Fourier transform technique, which reduces the simulation time required to obtain a converged spectrum. This method is widely used in magnetic resonance spectroscopy to treat noisy spectra with low resolution,[61,62] and Padé approximants have also been used in real-time electronic structure calculations.[63–65]

To use the Padé technique, the quantity $\mu_\lambda(\omega)$ in Eq. (10) is viewed as a polynomial expansion in $z = \exp(-\mathrm{i}\omega\Delta t)$:

$$\mu_\lambda(\omega) = \sum_{k=0}^{M} z^k \mu_\lambda(t_k) \quad (11)$$

This power series is then approximated using rational functions whose numerator and denominator are both power series expansions of a certain order. Taking the polynomial order to be $P = M/2$, Eq. (11) is equivalent to

$$\sum_{k=0}^{M} c_k z^k \sum_{m=0}^{P} b_m z^m = \sum_{k=0}^{P} a_k z^k \ . \quad (12)$$

We take $b_0 = 1$ by convention, thus Eq. (12) consists of $2P$ equations for a total of $2P$ variables ($\{a_i\}$ and $\{b_i\}$), which are solved by separating the equations according to orders in z. In matrix form, the solution for the coefficient $\{b_i\}$ is

$$\mathbf{b} = \mathbf{G}^{-1}\mathbf{d} \quad (13)$$

where $d_k = -c_{P+k}$ and $\mathbf{G}$ is a $P \times P$ matrix with $G_{km} = c_{P-m+k}$. The coefficients $\{a_i\}$ are obtained from the $\{b_i\}$:

$$a_k = \sum_{m=0}^{k} b_m c_{k-m} \ . \quad (14)$$

Having $\mathbf{a}$ and $\mathbf{b}$, the Fourier transform of $\mu_\lambda(\omega)$ can be constructed, and the result is that a shorter time sequence of input data is required to obtain a converged Fourier transform. In contrast to the Padé-accelerated transform technique that was introduced in Ref. 65, which introduces a representation based on occupied–virtual function pairs $\psi_i(\mathbf{r}, t)\, \psi_a(\mathbf{r}, t)$, the version that we have implemented transforms only the total dipole moment in Eqs. (10) and (11).

To demonstrate the technique and to check convergence with respect to total simulation time, we calculated the absorption spectrum of the methionine molecule at the oxygen K-edge (Fig. 1). Two different simulations are shown, using either $\Delta t = 0.01$ a.u. or $\Delta t = 0.02$ a.u., both of which are well within the Nyquist limit for this spectral range, which imposes a bound $\Delta t \leq 0.16$ a.u. at $E_{\max} = 540$ eV. Comparing a normal fast Fourier transform (FFT) of the time series $\mu_\lambda(t_k)$ with a Padé-accelerated transform, we find that the Padé technique produces a much better-converged spectrum in only half the simulation time, $t_{\max} = 600$ a.u. (≈ 14.5 fs). Near-edge features are converged with as little as one-quarter of that time. For simulations with $t_{\max} \leq 300$ a.u., clear artifacts are evident at higher energies, which diminish but do not disappear as the time step is reduced. These features provide a diagnostic to indicate that additional simulation time is required in order to converge the spectrum in a given energy range. Similar data for an ion-pair

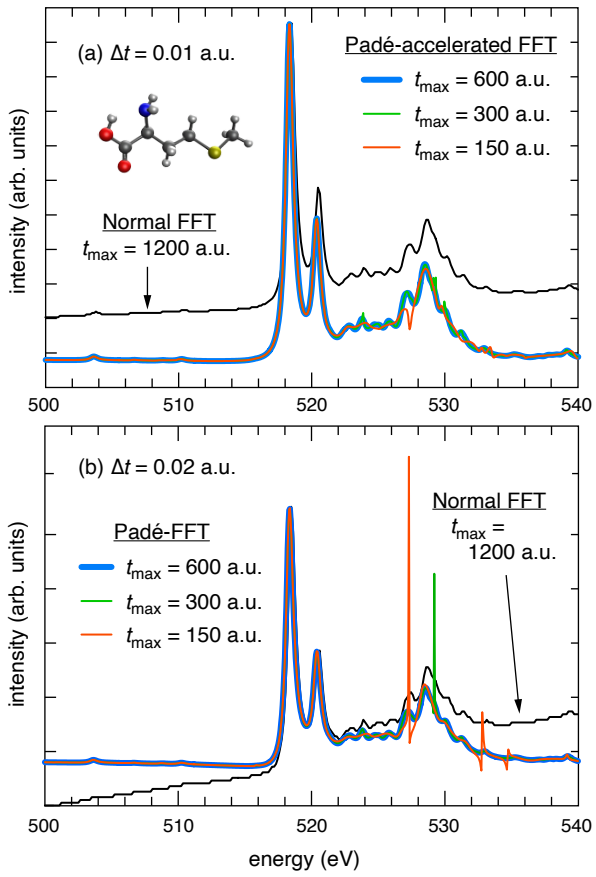

Fig. 1: Absorption spectrum of methionine at the oxygen K-edge [B3LYP/6-31+G(d) level], using (a) $\Delta t = 0.01$ a.u. versus (b) $\Delta t = 0.02$ a.u., for various propagation times $t_{\max}$. Simulation were initiated with a δ-function perturbation, ($\bar{\mathcal{E}}_x = \bar{\mathcal{E}}_y = \bar{\mathcal{E}}_z = 10^{-4}$ a.u.). In the Padé-accelerated case, the spectra computed using $t_{\max} = 1200$ a.u. are indistinguishable from the ones using $t_{\max} = 600$ a.u. that are shown.

dimer that will be considered below are shown in Fig. S1, demonstrating the appearance of artifacts in nitrogen K-edge spectra for $t_{\max} = 200$ a.u., which are not present for $t_{\max} = 600$ a.u.. For this reason, the TDKS simulations presented below use at least 600 a.u. of simulation time, in order to clearly elucidate all spectral features of this method. In Section 4 C 1, we will consider whether meaningful near-edge features can be extracted from shorter simulations.

2.A.4. Dipole moment filtering. It will be useful to decompose broadband TDKS spectra according to contributions arising from individual occupied orbitals, or small groups thereof, such as the two O(1s) orbitals in the methionine molecule of Fig. 1. To do so, we employ the dipole filtering technique that was introduced in Ref. 46, which we briefly recapitulate here.

We first recognize that

$$\mu_\lambda(t) = \mathrm{tr}\big[\mathbf{P}(t)\,\mathbf{D}_\lambda(t)\big] \tag{15}$$

in any orthonormal basis, where $\mathbf{D}_\lambda$ is the matrix representation of the dipole moment operator $\hat{\mu}_\lambda$. (In practice we will use the time-evolving MO basis.) We can separate

$$\mu_\lambda(t) = \sum_k^{\mathrm{occ}} \mu_{\lambda,k}(t) \tag{16}$$

into a sum of contributions from each occupied MO, by filtering out all contributions to $\mathbf{D}_\lambda(t)$ except for those arising from $\psi_k(\mathbf{r},t)$. In practice this means defining

$$\mu_{\lambda,k}(t) = \mathrm{tr}\big[\mathbf{P}(t)\,\mathbf{D}_{\lambda,k}(t)\big]\ , \tag{17}$$

where the matrix $\mathbf{D}_{\lambda,k}(t)$ consists of the kth row and column of $\mathbf{D}_\lambda(t)$ only, with zeros elsewhere.

The time-series data $\mu_{\lambda,k}(t)$ admit a Fourier representation analogous to Eq. (10), to which one may apply Padé approximants in the same way. The corresponding Fourier transform, $\mu_{\lambda,k}(\omega)$, affords a spectrum that can be associated with occupied MO ψ_k. According to Eq. (16) and the linearity of the Fourier transform, the sum of these orbital-indexed spectra must afford the parent TDKS spectrum, but various partitions of the sum in Eq. (16) might be considered. In the present work, we will always sum together all MOs corresponding to a given elemental edge, meaning for example the two O(1s) orbitals or the four C(1s) orbitals in the methionine molecule will be considered as a group and not decomposed any further.

One important implementation note bears pointing out. Density matrices $\mathbf{P}(t)$ at each time step are not retained, as these would represent an intractable amount of storage for most calculations. As a result, while there is virtually no overhead for computing arbitrary partitions of the sum in Eq. (16), the decision of which partitions to examine must be made at the outset. New partitions cannot be examined in post-processing. However, it would be possible to store dipole moment data $\mu_{\lambda,k}(t)$ for each individual MO ψ_k, in which case arbitrary partitions could be assembled after-the-fact.

2.B. Linear response theory. For completeness and to fix notation, we briefly recapitulate the LR-TDDFT formalism.[20] This arises from considering the first-order response of Eq. (4) to a weak perturbation,[23] therefore LR-TDDFT may be regarded as the weak-field limit of TDDFT. Identical spectra are obtained with the TDKS approach when the perturbing field is small and the time-dependent simulation is propagated for a sufficiently long time.[44,45]

The LR-TDDFT equation for excitation energies (ω) is

$$\begin{pmatrix} \mathbf{A} & \mathbf{B} \\ \mathbf{B}^\dagger & \mathbf{A}^\dagger \end{pmatrix} \begin{pmatrix} \mathbf{x} \\ \mathbf{y} \end{pmatrix} = \omega \begin{pmatrix} -\mathbf{1} & \mathbf{0} \\ \mathbf{0} & \mathbf{1} \end{pmatrix} \begin{pmatrix} \mathbf{x} \\ \mathbf{y} \end{pmatrix}\ , \tag{18}$$

where the matrices **A** and **B** are Hessians with respect to orbital rotations,[20] given by

$$A_{ia,jb} = (\varepsilon_a - \varepsilon_i)\delta_{ij}\delta_{ab} + \frac{\partial F_{ia}}{\partial P_{jb}} \tag{19a}$$

$$B_{ia,jb} = \frac{\partial F_{ia}}{\partial P_{bj}} \, . \tag{19b}$$

Indices i and j refer to occupied MOs whereas a and b indicate virtual MOs. All calculations reported here invoke the Tamm-Dancoff approximation,[20] which simplifies Eq. (18) by neglecting the de-excitation amplitudes **y**. (These are typically $\sim 100\times$ smaller than the largest **x** amplitudes.) The matrix **B** is absent from the resulting eigenvalue problem, which is

$$\mathbf{A}\mathbf{x} = \omega\mathbf{x} \, . \tag{20}$$

This approximation has little effect on XAS spectra (see Fig. S2a) and is used for all other LR-TDDFT calculations reported herein.

The LR-TDDFT formalism has been adapted for the calculation of core excitation spectra using frozen occupied orbitals,[5,26,66–68] equivalent to what is sometimes called the CVS approximation.[1,30,31,34] This corresponds to neglecting amplitudes x_{ia} in Eq. (20) unless i is a core orbital of interest, *e.g.*, O(1s) or C(1s). Each elemental K-edge is computed separately, using the full virtual space (all ψ_a) but including only the occupied orbitals ψ_i for that particular elemental edge. An example for the oxygen K-edge of methionine (Fig. S2b) demonstrates that this involves negligible approximation, consistent with the general validity of the CVS approximation for K-edge excitations.[36]

3 Computational Methods

All calculations presented here were obtained using a locally-modified version of Q-Chem v. 6.0,[8] in which we have implemented dipole filtering based on a previous implementation of the TDKS method.[55] We will analyze the veracity of TDKS spectra in Section 4, but first we present computational details (Section 3 A) and basis-set testing (Section 3 B).

3.A. Functionals and numerical parameters. We set $\Delta t = 0.02$ a.u. for all calculations at the oxygen, nitrogen, and carbon K-edges, which should be adequate even by very conservative convergence estimates that are stricter than the Nyquist frequency.[45] Tests using time steps as small as $\Delta t = 0.001$ a.u. demonstrate that oxygen K-edge spectra are converged (Fig. S3). The method of Padé approximants is used to post-process all of the dipole moment data from TDKS simulations. Exponential damping is applied to the time series $\mu_\lambda(t)$, with a damping constant corresponding to spectral broadening of 0.7 eV. As discussed in Section 2 A 3, most of the TDKS spectra reported below are based on $t_{\max} = 600$ a.u. (≈ 14 fs) of propagation time. Whether shorter propagation times can be used in practical calculations is considered in Section 4 C 1.

Starting from a ground-state SCF calculation, converged to a threshold of 10^{-8} Ha, the density is perturbed using a δ-function pulse in which the external field is only nonzero during the first two time steps. To normalize the initial perturbation across different choices of Δt, we follow Ref. 55 and report the *integrated* electric field strength $\bar{\boldsymbol{\mathcal{E}}}$, whose components are

$$\bar{\mathcal{E}}_\kappa = \mathcal{E}_\kappa \Delta t \tag{21}$$

for $\kappa \in \{x, y, z\}$. Here, $\mathcal{E}_\kappa$ is the actual field amplitude in the sense of Eq. (8) but that quantity is not needed to compute the absorption spectrum $S(\omega)$. The perturbing field consists of equal components in each Cartesian direction ($\bar{\mathcal{E}}_x = \bar{\mathcal{E}}_y = \bar{\mathcal{E}}_z$), which ensures that the perturbation creates a superposition of all excited states regardless of electronic symmetry. We set $\bar{\mathcal{E}}_\kappa = 10^{-4}$ a.u. for all calculations reported here. Integral screening and shell-pair drop tolerances are set to 10^{-12} a.u..

Some basis-set testing is presented in Section 3 B. These tests, and many of the spectra presented in Section 4, are computed using "short-range corrected" (SRC) density functionals known as SRC1 or SRC2.[69,70] These are range-separated hybrid functionals based on the short-range exchange functional μBLYP,[71,72] parameterized specifically for LR-TDDFT calculations at elemental K-edges.[69,70] These functionals use a large fraction of exact exchange that is attenuated on a length scale of < 1 Å,[69] which presumably corrects for differential self-interaction error between the core and valence virtual orbitals. Actually there are two versions of both functionals, SRCn-r1 and SRCn-r2,[4] where the former are parameterized for "first-row" elements (C, N, O, etc.) and contains 50% (SRC1) or 55% (SRC2) short-range Hartree-Fock exchange, whereas the "second-row" versions (SRCn-r2) contain 87% (SRC1) and 91% (SRC2) short-range Hartree-Fock exchange. The SG-1 numerical quadrature grid[73] is used to integrate the exchange-correlation functional.

Although the SRC functionals prove to be very accurate for LR-TDDFT calculations (and thus for TDKS calculations), this appears to benefit from significant error cancellation as these functionals perform exceedingly poorly in ΔSCF calculations.[74,75] As such, we have begun to shift our emphasis back to functionals such as B3LYP that perform well the ΔSCF approach.[74,75] LR-TDDFT calculations with B3LYP are often significantly shifted with respect to experiment (by > 10 eV in some cases),[69,70,76–79] yet relative peak positions and chemical shifts exhibit accuracy on par with many-body methods.[80] This observation is consistent with ΔSCF results.[75] Relativistic corrections are not included in this work, as these are estimated to be ≈ 0.5 eV for oxygen and even smaller for lighter elements.[81–83]

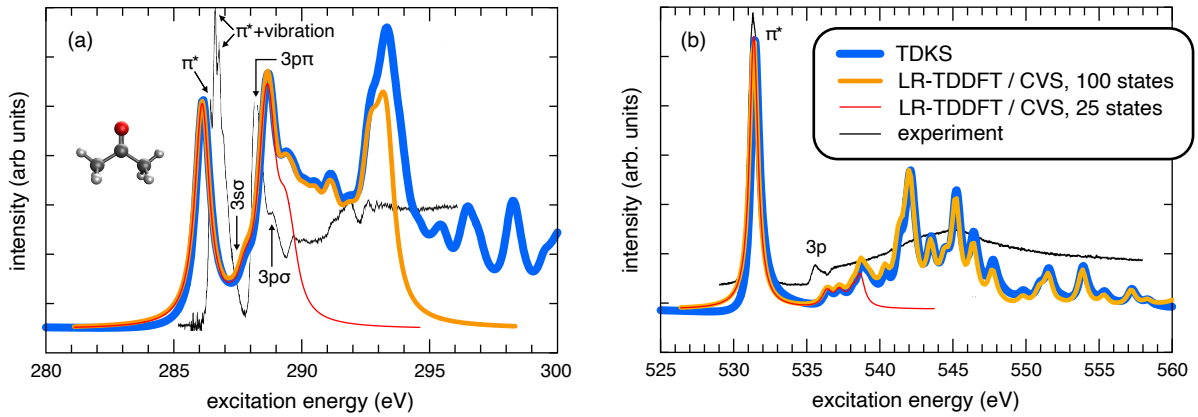

Fig. 2: Absorption spectra of acetone molecule at (a) the carbon K-edge and (b) the oxygen K-edge, computed at the SRC1-r1/ 6-311(2+,2+)G(d,p) level and compared to experimental spectra that are reproduced from Ref. 84. LR-TDDFT excitation energies are computed using a CVS active space consisting of the three C(1s) MOs, or the O(1s) MO, along with all of the virtual MOs; each transition is broadened using a Lorentzian function with a 0.7 eV width. The TDKS calculation ($\bar{\mathcal{E}}_\kappa = 10^{-4}$ a.u., $\Delta t = 0.02$ a.u., $t_{\max} = 600$ a.u.) was converged using Padé approximants, then scaled to match the LR-TDDFT intensity for the first absorption peak. Relativistic effects (not included here) would shift the calculated spectra to higher energy by ≈ 0.1 eV.[81–83] State assignments for low-lying transitions are taken from Ref. 84.

3.B. Tests of basis sets and active spaces. Several previous studies have explored modified Gaussian basis sets for use in XAS calculations.[85–89] In some cases, standard Gaussian basis sets have been "uncontracted",[85–87] meaning that each Gaussian primitive is used as an independent basis function, thus improving the variational flexibility of the core functions. A separate strategy[87–89] is to use basis sets that include core–valence polarization functions, such as cc-pCVXZ.[90] It has been suggested that these basis sets work well for core-level spectroscopy precisely because the additional polarization functions are uncontracted.[88]

In contrast to the behavior observed using correlated wave functions,[86,89] our testing with LR-TDDFT reveals that uncontracting the basis sets modifies the near-edge excitation energies by < 0.1 eV and modifies spectra hardly at all, even at much higher excitation energies (Fig. S4). These tests include the basis sets 6-31+G(d), 6-311(2+,2+)G(d,p), (aug-)cc-pVTZ, aug-cc-pCVTZ, and def2-TZVPD. A previous LR-TDDFT study also concluded that basis set effects are rather small for XAS calculations,[87] although these effects are somewhat more pronounced for x-ray emission,[87] because the reference state for LR-TDDFT involves core ionization in that case.[91] (Emission spectra are not considered in the present work.) A summary of basis set effects is presented in Table S1, demonstrating that the SRC functionals predict oxygen and carbon K-edge excitation energies within 0.1–0.2 eV of experiment for small organic molecules. Those deviations are of the same magnitude (or smaller) than relativistic corrections for second-row elements.[81–83] All LR-TDDFT calculations reported below were performed using the CVS approximation. Excitation energies were broadened using a Lorentzian function with a width of 0.7 eV, in order to be directly comparable to spectra obtained from TDKS simulations.

4 Results and Discussion

Our major results consist in comparing x-ray spectra obtained using TDKS simulations to those obtained using LR-TDDFT, with the latter calculations performed within the CVS approximation. Some basic comparisons can be found in Section 4 A, following which we describe the use of dipole filtering to identify and remove continuum artifacts in the TDKS spectra (Section 4 B). Finally, some chemically relevant examples are considered in Section 4 C.

4.A. Comparison of TDKS to LR-TDDFT. Good agreement between LR-TDDFT and TDKS spectra has been demonstrated previously for valence excitation spectra,[44,45] however the situation is more complicated for core-level spectra. We begin by comparing these two implementations of TDDFT for XAS of simple organic molecules, such as acetone at the carbon or oxygen K-edge as depicted in Fig. 2. LR-TDDFT/ CVS spectra are shown, based on either 25 or 100 excited states, although the smaller number is sufficient to reproduce the near-edge features. (Throughout this work, we apply 0.7 eV Lorentzian broadening to the LR-TDDFT excitation energies, to obtain a spectrum that can be easily compared to the TDKS result.) Agreement between LR-TDDFT and TDKS is quantitative provided that enough states are included in the LR-TDDFT calculation. The agreement with experiment[84] is also quite

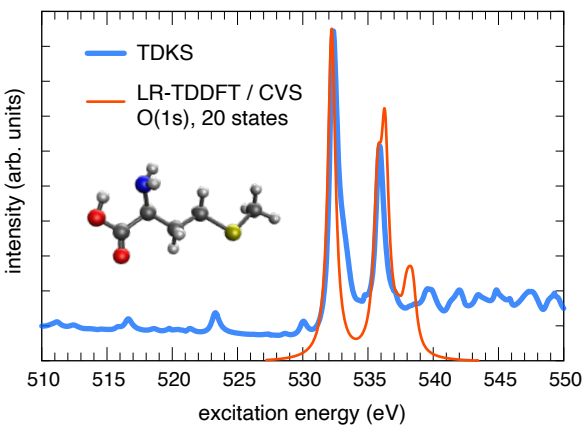

Fig. 3: TDDFT (SRC1-r1/def2-TZVPD) spectra of methionine at the oxygen K-edge. Real-time simulations were propagated for $t_{\max} = 300$ a.u. using $\Delta t = 0.02$ a.u., following a δ-function impulse with $\bar{\mathcal{E}}_x = \bar{\mathcal{E}}_y = \bar{\mathcal{E}}_z = 10^{-4}$ a.u.. Padé approximants were used to accelerate convergence of the Fourier transform. The LR-TDDFT calculation used an active space consisting of both O(1s) occupied MOs along with all of the virtual MOs, with Lorentzian broadening (0.7 eV), and the baseline is offset for clarity. Features below 531 eV in the TDKS spectrum correspond to N(1s) $\rightarrow$ continuum transitions.

good for the near-edge features, because we use the parameterized SRC1-r1 functional along with a basis set of reasonable quality. At higher excitation energies, resonances are too shorted-lived to be observed and the experimental spectrum becomes featureless. Structure persists in the TDDFT spectra because all states have infinite lifetimes due to the use of a compact basis set. In reality, then, the only meaningful part of the spectra in Fig. 2 is encompassed by about 25 discrete transitions.

For the acetone molecule it is possible to compare the TDKS spectrum directly to LR-TDDFT results without post-processing, but this becomes more difficult for larger molecules, especially in high-quality basis sets. This is demonstrated in Fig. 3 for the methionine molecule at the SRC1-r1/def2-TZVP level. In this case, the TDKS spectrum predicts an intense peak at 532 eV, in quantitative agreement with the O(1s) $\rightarrow$ LUMO transition from a LR-TDDFT/CVS calculation, but several low-intensity "pre-edge" features appear below this. These features are missing from the LR-TDDFT spectrum, indicating that they do not originate from O(1s) orbitals. Instead, they correspond to excitations from N(1s) orbitals into the highest-energy virtual MOs. (The latter are orthogonalized discretized continuum states rather than valence virtual orbitals.[92]) The nature of these quasi-unbound excitations becomes clear if one computes all $o \times v$ states afforded by the LR-TDDFT eigenvalue problem in Eq. (20), which is feasible for very small molecules in small basis sets. Examining this complete set of transitions, one finds a semi-continuous sequence of states that connects each of the x-ray K-edges (carbon, nitrogen, oxygen, ...), as shown in Fig. S5. These are core $\rightarrow$ continuum excitations, which are called are called "intruder states" in Ref. 65. They ought to have exceeding small lifetimes but are bound in the TDKS calculation by the finite basis set. In the small basis sets where one can afford to compute all $o \times v$ states (as in Fig. S5), these transitions to the continuum mostly have very small oscillator strengths, but results below demonstrate that they can acquire significant intensity in higher-quality basis sets.

The spurious pre-edge features in Fig. 3 are perhaps easy to identify as such, and therefore to discount, but this may not be true in more complex systems. For example, metal–ligand hybridization in organometallic systems can provide an intensity borrowing mechanism leading to the appearance of weakly-allowed 1s $\rightarrow$ 3d pre-edge transitions.[93] Even for main features in the methionine spectrum in Fig. 3, agreement between LR-TDDFT and TDKS is less quantitative than what we observed previously for acetone. This is a direct reflection of the appearance of N(1s) $\rightarrow$ continuum transitions in the TDKS spectrum that are excluded from the LR-TDDFT spectrum by virtue of the active space that is used to model the oxygen K-edge.

The appearance of spurious transitions to the continuum can be avoided in TDKS simulations via *ad hoc* replacement of positive SCF eigenvalues (representing unbound states) with complex-valued eigenvalues in the MO representation of $\mathbf{P}(t)$.[58,59] This transformation has the effect of giving those states a finite lifetime that can be made arbitrarily short by selecting the imaginary part of the eigenvalue. An alternative approach would be to introduce a complex absorbing potential.[55] However, both methods have some arbitrary parameters that must be adjusted, potentially on a case-by-case basis, and we have not pursued either method in this work. Instead, we turn to dipole filtering as a diagnostic to understand the origins of various features in a given TDKS spectrum.

4.B. Continuum artifacts. Figure 4 presents TDKS spectra for methionine, using the SRC1-r1 functional in four different basis sets, in the region from 500–550 eV. LR-TDDFT/CVS calculations suggest that the O(1s) $\rightarrow$ LUMO transition should be found at $\approx$ 532 eV for this functional and these basis sets, but the TDKS spectra have pronounced features at lower excitation energies. The oxygen K-edge spectrum can be extracted from the TDKS results by filtering on the O(1s) orbitals. In a small basis set such as 6-31+G(d), this has virtually no effect on the spectrum within the indicated energy range (Fig. 4a), and the first peak that is observed is in fact the O(1s) $\rightarrow$ LUMO transition, at 531.9 eV. As such, the issue of pre-edge artifacts in TDKS spectra may go unnoticed if low-quality basis sets are used. With the benefit of hindsight, one can just barely make out two very small pre-edge features at 520.6 and 527.4 eV in the SRC1-r1/6-31+G(d) spectrum, although these might

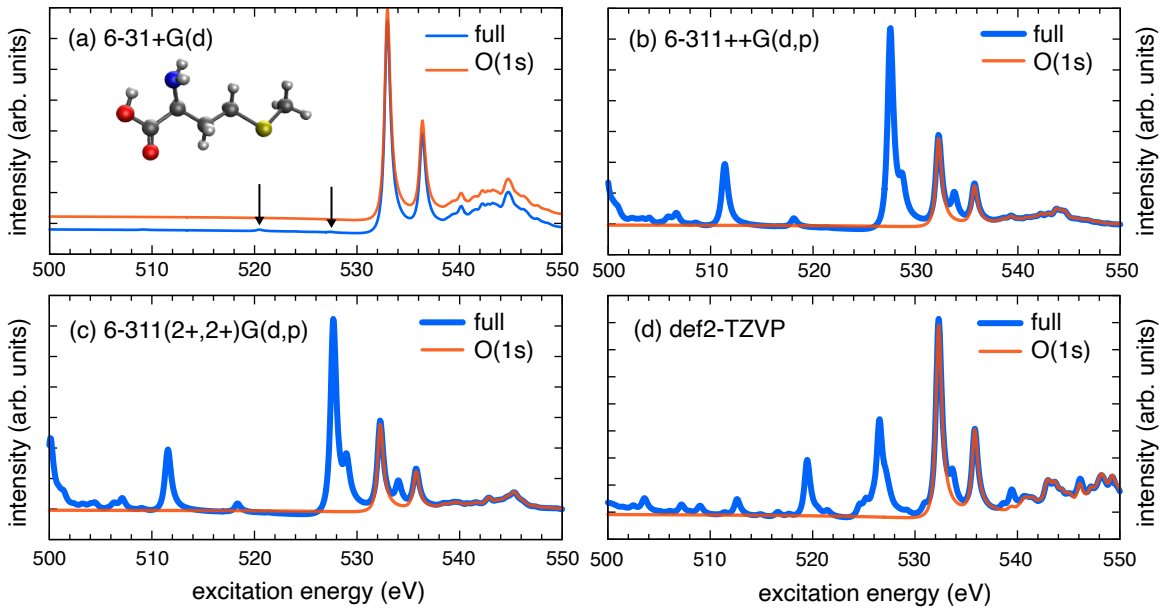

Fig. 4: TDKS absorption spectra for methionine computed using the SRC1-r1 functional in various basis sets. All simulations used Padé approximants with $t_{\max} = 600$ a.u. and $\Delta t = 0.02$ a.u., following a δ-function impulse with $\bar{\mathcal{E}}_x = \bar{\mathcal{E}}_y = \bar{\mathcal{E}}_z = 10^{-4}$ a.u.. Spectra labeled as "full" are based on the complete dipole moment function whereas those labeled "O(1s)" exclude all contributions to $\mathbf{D}_\lambda(t)$ except for those originating with the two O(1s) orbitals. The O(1s) spectrum in (a) has been shifted to better reveal the baseline in both spectra, and the arrows highlight two very small pre-edge features.

easily have been written off as noise in the absence of results in larger basis sets.

In triple-ζ basis sets the artifacts can no longer be ignored. For example, in the full TDKS spectrum computed at the SRC1-r1/6-311++G(d,p) level (Fig. 4b), it is difficult to tell (in the absence of LR-TDDFT calculations) whether the oxygen K-edge lies at 528 eV or at 532 eV. The peak at 528 eV disappears in the filtered O(1s) spectrum, however, suggesting that this feature is an artifact of N(1s) $\rightarrow$ continuum transitions. That assignment is confirmed by filtering on the N(1s) orbital, whereas the feature at 511 eV arises from S(2p) orbitals as seen in Fig. 5a.

Spectra in Fig. 5 are decomposed into elemental contributions, for calculations using two different basis sets. In each case, the "full" TDKS spectrum is recovered as a sum of contributions from O(1s), N(1s), and S(2p) orbitals, although a very small contribution from S(2s) orbitals is omitted from Fig. 5a, for clarity. Note that relativistic corrections, which are omitted in this work, are much larger for third-row atoms, *e.g.*, 5.9 eV for sulfur[81] versus 0.5 eV for oxygen.[82,83] If included, these effects would therefore shift the S(2p) feature in Fig. 5a by 5.4 eV but this would not fundamentally alter the picture described here, where transitions to the continuum contaminate spectra at the desired elemental edges, in an erratic manner that is highly sensitive to the choice of basis set.

Juxtaposition of spectra from two different basis sets in Fig. 5 makes it clear that basis-set effects on the O(1s) $\rightarrow$ LUMO feature at 532 eV are rather small, consistent with the testing reported in Section 3 B. In contrast, the N(1s) $\rightarrow$ continuum transitions are extremely sensitive to the choice of basis, which is a general characteristic of continuum states in Gaussian basis sets.[92] At the SRC1-r1/6-311++G(d,p) level there is a continuum feature just below the oxygen K-edge that is significantly more intense than the O(1s) $\rightarrow$ LUMO transition, and the two features might easily be confused, whereas at the SRC1-r1/def2-TZVPD level the N(1s) $\rightarrow$ continuum transitions manifest as a small pre-edge feature. In view of these and other artifacts, and in the absence of filtering, there is no way to be confident in the assignment of the K-edge transition, given the large peak shifts that often characterize XAS calculations using TDDFT.[69,70,76–79]

4.C. Chemically relevant examples. Having seen that dipole filtering is essential to remove continuum artifacts in broadband TDKS spectra, we next discuss some chemically-motivated examples where unfiltered spectra (in realistic basis sets) obscure key information.

4.C.1. Ionic liquid ion pair. Our first example is an ion-pair dimer, 1-butyl-3-methylimidazolium ($C_4C_1Im^+$) and thiocyanate (SCN^-), representing a typical dialkylimidazolium ionic liquid.[94] This and other room-temperature ionic liquids have been using NEXAFS spectroscopy at the nitrogen and sulfur K-edges.[95] In ac-

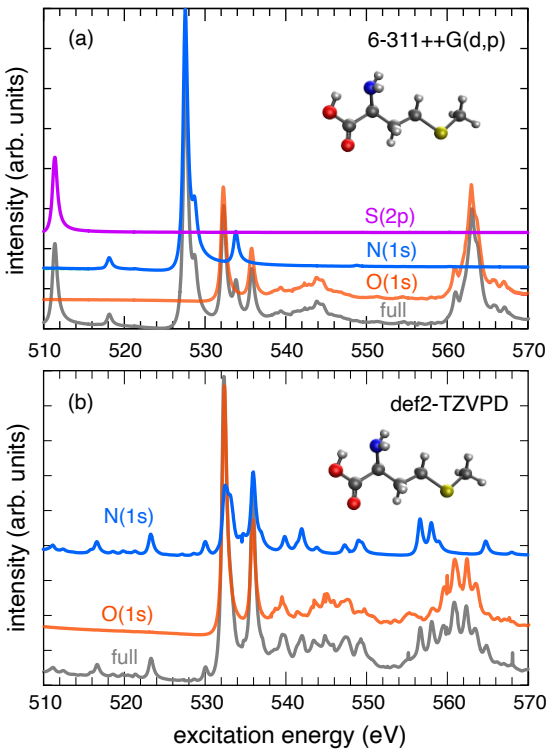

Fig. 5: TDKS absorption spectra for methionine computed using the SRC-r1 functional with (a) the 6-311++G(d,p) and (b) the def2-TZVPD basis set. Simulations are based on $t_{\max} = 300$ a.u. with other parameters as described in Fig. 4. The complete TDKS spectrum ("full") is compared to filtered spectra involving only the O(1s), N(1s), or S(2p) orbitals, as indicated. The spectra have been shifted vertically for clarity but they share a common intensity scale such that the sum of the filtered spectra equals the full spectrum. which follows from Eq. (16).

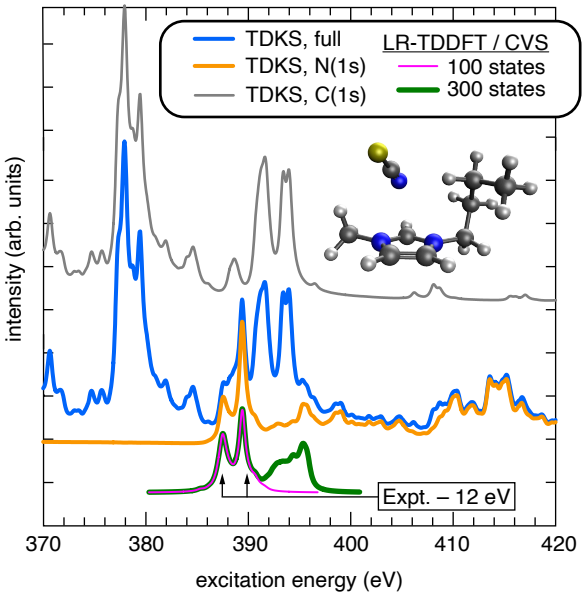

Fig. 6: Absorption spectra near the nitrogen K-edge for the ionic liquid dimer $[C_4C_1Im][SCN]$, computed at the SRC1-r1/6-311(2+,2+)G(d,p) level using the simulation parameters described in Fig. 4. Experimental peak maxima are from Ref. 95.

companying calculations it was found that excited states could be delocalized across the ion pair in some cases,[95] such that the computational modeling should not be limited to the individual cations and anions.

Spectra shown in Fig. 6 for one particular structure of $[C_4C_1Im][SCN]$ were computed at the SRC1-r1/6-311(2+,2+)G(d,p) level of theory, mirroring LR-TDDFT/CVS calculations reported previously.[95] Absent the filtering step, the TDKS spectrum is simply uninterpretable as there is significant contamination from C(1s) $\rightarrow$ continuum excitations. Interloper states contribute spurious (albeit high-intensity) pre-edge features but also overlap with the nitrogen K-edge itself. Upon filtering, a good match is obtained to LR-TDDFT/CVS results, with the nitrogen K-edge appearing at 387.5 eV with a second peak at 389.4 eV. Experimentally, these two features appear at 399.5 eV and 401.9 eV (although they are quite broad),[95] so the spectra in Fig. 6 must be shifted by about 12 eV to match. However, the chemical shift between the two peaks is predicted more accurately: 1.9 eV (theory) versus 2.4 eV (experiment). Note that the $[C_4C_1Im][SCN]$ dimer exhibits conformation-dependent spectral shifts up to ~ 1 eV,[95] and we have not attempted any conformational search here.

The filtered TDKS spectrum is a good match to the LR-TDDFT/CVS result but it is important to consider the cost of either calculation. To do this, we first interrogate the simulation length ($t_{\max}$) that is required to obtain the experimental feature. The TDKS spectrum shown in Fig 6 is a well-converged result based on $t_{\max} = 600$ a.u. (≈ 14.5 fs) of simulation time, and in Fig 7 we recompute this spectrum based on successively shorter simulations, down to $t_{\max} = 75$ a.u. (≈ 1.8 fs). Artifacts can certainly be observed in spectra obtained from shorter-time simulations, including negative intensities at some excitation energies, and the unfiltered spectra obtained at different values of $t_{\max}$ differ significantly from one another. Upon dipole filtering, however, the two peaks that characterize the nitrogen near-edge can be observed even for the shortest simulation. In fact, these peaks shift only by ~ 0.1 eV from $t_{\max} = 75$ a.u. to $t_{\max} = 600$ a.u.. Monitoring the filtered spectrum thus provides an incisive convergence metric whereas the the unfiltered spectrum does not.

If the simulation time is reduced by another factor of two ($t_{\max} = 37.5$ a.u.) then the peaks that constitute the near-edge merge together as shown in Fig. S6; therefore, we take $t_{\max} = 75$ a.u. to be the minimum simulation length required for this particular application. At the SRC1-r1/6-311(2+,2+)G(d,p) level, this calculation involves 479 basis functions and the TDKS simulation requires 2.5 h (wall time) on a single compute node

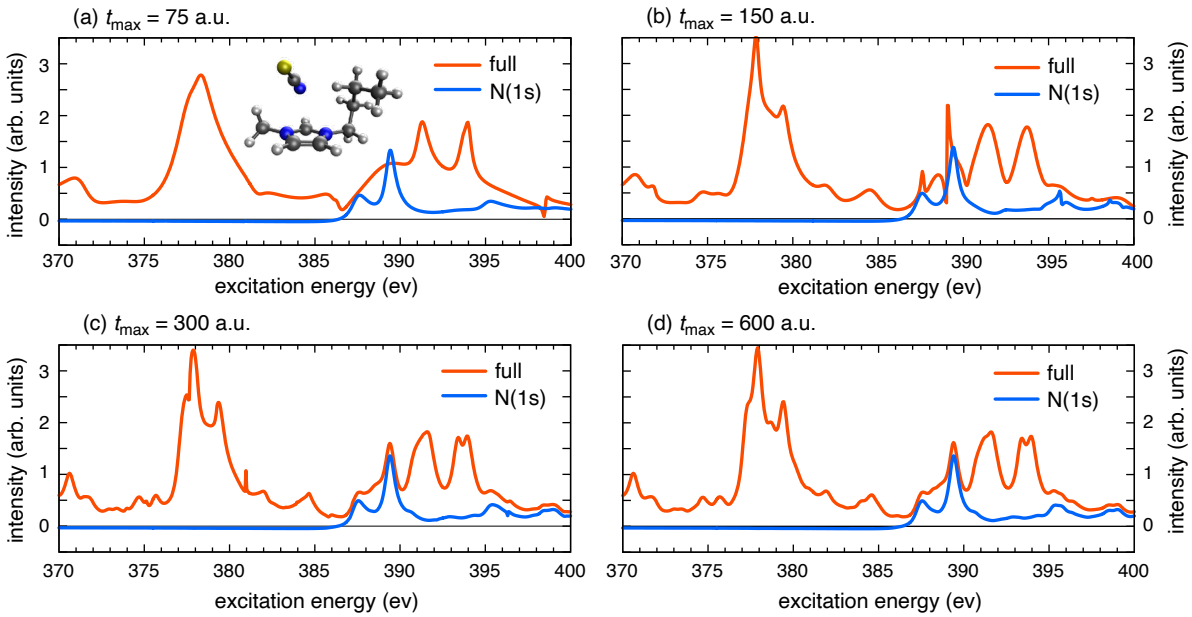

Fig. 7: TDKS absorption spectra near the nitrogen K-edge for $[C_4C_1Im][SCN]$ (shown), computed at the SRC1-r1/6-311(2+,2+)G(d,p) level, for simulations using (a) t_{max} = 75 a.u., (b) t_{max} = 150 a.u., (c) t_{max} = 300 a.u., and (d) t_{max} = 600 a.u.. (Further reduction in simulation time merges the two near-edge features.) Other simulation parameters are the same as those described in Fig. 4 and the spectrum for t_{max} = 600 a.u. is the same as that shown in Fig. 6.

using 40 processor cores, or 100.6 h of aggregate computing time. (We have argued that aggregate computing time should be the measure of cost that is reported in high-performance computing.[96–98]) By contrast, LR-TDDFT/CVS calculations with 100 and 300 roots require only 14 and 35 min, respectively, on just 20 cores of the same hardware. For the calculation with 300 states, this is 11.7 h of aggregate computing time, or 12% of the TDKS cost. Note that frozen virtual orbital approximations (not used here) can further accelerate LR-TDDFT calculations,[67,68] whereas no such approximation is available for TDKS simulations.

4.C.2. TiO_2. We next consider the isolated TiO_2 molecule as a very simple example of a transition metal oxide. This is an interesting case because the metal L-edge overlaps with the oxygen K-edge in these non-relativistic calculations. In general, L-edge spectra require the treatment of spin-orbit coupling, to describe the splitting of the 2p states into $2p_{3/2}$ and $2p_{1/2}$,[3,35,99] but this is not considered in the present work where our goal is simply to compare TDKS and LR-TDDFT results and to emphasize the necessity of dipole filtering in the TDKS case.

Figure 8 plots TiO_2 excitation spectra in the range 500–550 eV, computed at the SRC1-r1/def2-TZVPD level. Given the large shifts that are often required to match experiment in TDDFT calculations, it is not obvious which feature in the full TDKS spectrum is the O(1s) → LUMO transition. For example, we have seen above that the SRC1-r1 functional places the oxygen K-edge at around 532 eV, but if this same TiO_2 calculation is performed at the B3LYP/def2-TZVPD level, the O(1s) → LUMO excitation appears at 515 eV and there is a band of transitions between 515–520 eV. There are prominent features in the same energy region in the TDKS spectra shown in Fig. 8, but dipole filtering reveals that they are not associated with the oxygen K-edge. Instead, the most intense absorption feature in Fig. 8 is associated with excitation from Ti(2p) orbitals. In this example the oxygen K-edge, which (as in previous examples) appears around 532 eV for the SRC1-r1 functional, includes significant contamination from the titanium L-edge. This contamination, involving excitations originating in the Ti(2p) orbitals, is easily filtered away to expose separate oxygen and titanium spectra, either of which is a good match to the corresponding LR-TDDFT/CVS calculation.

In the L-edge case, the CVS active space consists of Ti(2p) orbitals only, along with the full virtual space. LR-TDDFT/CVS calculations based on this active space are in quantitative agreement with the corresponding features in the TDKS calculation as demonstrated in Fig 8b. Note that even when dipole filtering is applied, the TDKS simulation is based on a time-evolving density matrix that includes all of the occupied MOs at every time step. As such, the quantitative agreement with LR-TDDFT/CVS calculations that we document here demonstrates that there is essentially no error in the CVS approximation for this example. This observation is significant, because whereas the CVS approximation has been carefully benchmarked for K-edge spectra,[36] less is known about

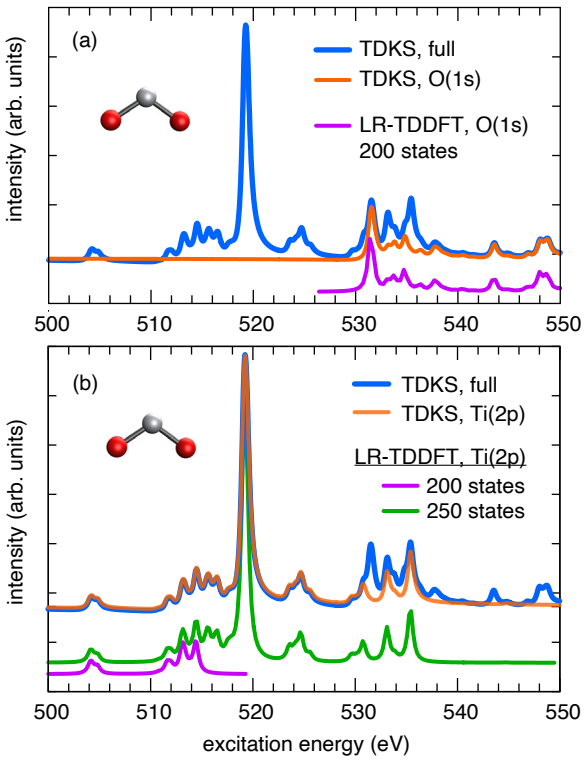

Fig. 8: Absorption spectra for the TiO_2 molecule computed using TDDFT at the SRC1-r1/def2-TZVPD level. Real-time simulations are based on $t_{\max} = 1200$ a.u. with other parameters as described in Fig. 4, and are filtered according to (a) the O(1s) orbitals, to obtain the oxygen K-edge, or else (b) Ti(2p) orbitals, revealing the titanium L-edge. LR-TDDFT spectra use the corresponding CVS active space consisting of either O(1s) or Ti(2p) orbitals plus the full virtual space. Vertical offsets have been added for clarity.

its accuracy for L- and M-edge spectra. In the latter cases, the nominal initial-state orbitals in the second and third shell may not be energetically well separated from other orbitals, leading to larger errors when the CVS approximation is applied. In principle, interior eigenvalue solvers[27–29] can be used to address the veracity of the CVS approximation in such cases, but this has so far been done only in a very limited way.[29] Although we do not see any evidence for a breakdown of the CVS approximation for the L-edge of TiO_2 molecule, the question is worth examining in larger systems. TDKS simulations provide a means to obtain spectra that do not invoke any active-space approximation.

Those benchmarks can be expensive, however. In the present example, the cost of LR-TDDFT remains considerably lower than that of TDKS even though several hundred individual excited states are required just to obtain the near-edge Ti(2p) features. For the Ti(2p) CVS active space, a calculation with $o = 3$ active orbitals and $v = 128$ virtual orbitals (which is the entire virtual space in the def2-TZVPD basis set) requires less than 3 min on 20 processors. LR-TDDFT calculations with a O(1s) active space required about 2 min. TDKS simulations, running on the same hardware, require 14.3 hours to reach $t_{\max} = 1200$ a.u.. Assuming that the near-edge features could be obtained using $t_{\max} = 75$ a.u., as for the $[C_4C_1Im][SCN]$ system considered above, then a more pragmatic calculation would require almost an hour an 20 processors. This does not include the time required for convergence testing.

5 Conclusions

We have examined the use of TDKS or "real-time" TDDFT simulations for core-level spectroscopy at various elemental K- and L-edges. At first glance, the TDKS approach seems attractive for this application. It allows all of the elemental x-ray edges to be computed at once, in a single broadband calculation, up to an energy scale that is varies inversely with the time step used to integrate the equations of motion. In practice, however, TDKS spectra are contaminated with transitions to the continuum, to the point that they are frequently uninterpretable. A post-processing filter restores interpretability by decomposing the full TDKS spectrum into components defined by subsets of the MOs, and meaningful NEXAFS spectra can be recovered. However, the cost remains an order of magnitude larger than conventional LR-TDDFT within a CVS-style active-space approximation that uses only the core MOs of interest. This is true despite the use of Padé approximants to process the TDKS data, which reduces the simulation time required to resolve the near-edge features to ≈ 2 fs.

Moving forward, we suggest that the utility of the TDKS approach for core-level spectroscopy may lie in the fact that it obviates the need to invoke a CVS approximation, which is (by contrast) essential in LR-TDDFT and other eigenvalue-based approaches to x-ray spectroscopy. At the DFT level, TDKS simulations may provide benchmarks to understand the assess the accuracy of active-space approximations, which remain relatively untested for x-ray spectroscopy at element L- and M-edges.

Supporting Information

Basis-set testing and convergence results.

Acknowledgments

This work was supported by National Science Foundation grant nos. CHE-1665322 and CHE-1955282. Calculations were performed at the Ohio Supercomputer Center.[100]

Author Declarations

J.M.H. serves on the board of directors of Q-Chem Inc.

Author Contributions

John M. Herbert: Conceptualization (lead); Data curation (equal); Formal analysis (lead); Funding acquisition (lead); Investigation (equal); Methodology (equal); Project administration (lead); Software (equal); Supervision (lead); Validation (equal); Visualization (lead); Writing – original draft (lead); Writing – review and editing (lead). **Ying Zhu:** Investigation (equal); Methodology (equal); Software (equal). **Bushra Alam:** Data curation (equal); Formal analysis (contributing); Investigation (equal); Methodology (contributing); Validation (equal); Visualization (contributing); Writing – original draft (contributing). **Avik Kumar Ojha:** Investigation (contributing); Data curation (contributing).

References

[1] P. Norman and A. Dreuw, "Simulating x-ray spectroscopies and calculating core-excited states of molecules", *Chem. Rev.*, **118**, 7208–7248 (2018).

[2] S. I. Bokarev and O. Kühn, "Theoretical x-ray spectroscopy of transition metal compounds", *WIREs Comput. Mol. Sci.*, **10**, e1433 (2020).

[3] J. M. Kasper, T. F. Stetina, A. J. Jenkins, and X. Li, "*Ab initio* methods for L-edge x-ray absorption spectroscopy", *Chem. Phys. Rev.*, **1**, 011304 (2020).

[4] N. A. Besley, "Density functional theory based methods for the calculation of x-ray spectroscopy", *Acc. Chem. Res.*, **53**, 1306–1315 (2020).

[5] N. A. Besley, "Modeling of the spectroscopy of core electrons with density functional theory", *WIREs Comput. Mol. Sci.*, **12**, e1527 (2021).

[6] C. D. Rankine and T. J. Penfold, "Progress in the theory of x-ray spectroscopy: From quantum chemistry to machine learning and ultrafast dynamics", *J. Phys. Chem. A*, **125**, 4276–4293 (2021).

[7] B. P. Klein, S. J. Hall, and R. J. Mauer, "The nuts and bolts of core-hole constrained *ab initio* simulation for K-shell x-ray photoemission and absorption spectra", *J. Phys.: Condens. Matt.*, **33**, 154005 (2021).

[8] E. Epifanovsky, A. T. B. Gilbert, X. Feng, J. Lee, Y. Mao, N. Mardirossian, P. Pokhilko, A. F. White, M. P. Coons, A. L. Dempwolff, Z. Gan, D. Hait, P. R. Horn, L. D. Jacobson, I. Kaliman, J. Kussmann, A. W. Lange, K. U. Lao, D. S. Levine, J. Liu, S. C. McKenzie, A. F. Morrison, K. D. Nanda, F. Plasser, D. R. Rehn, M. L. Vidal, Z.-Q. You, Y. Zhu, B. Alam, B. J. Albrecht, A. Aldossary, E. Alguire, J. H. Andersen, V. Athavale, D. Barton, K. Begam, A. Behn, N. Bellonzi, Y. A. Bernard, E. J. Berquist, H. G. A. Burton, A. Carreras, K. Carter-Fenk, R. Chakraborty, A. D. Chien, K. D. Closser, V. Cofer-Shabica, S. Dasgupta, M. de Wergifosse, J. Deng, M. Diedenhofen, H. Do, S. Ehlert, P.-T. Fang, S. Fatehi, Q. Feng, T. Friedhoff, J. Gayvert, Q. Ge, G. Gidofalvi, M. Goldey, J. Gomes, C. E. González-Espinoza, S. Gulania, A. O. Gunina, M. W. D. Hanson-Heine, P. H. P. Harbach, A. Hauser, M. F. Herbst, M. Hernández Vera, M. Hodecker, Z. C. Holden, S. Houck, X. Huang, K. Hui, B. C. Huynh, M. Ivanov, A. Jász, H. Ji, H. Jiang, B. Kaduk, S. Kähler, K. Khistyaev, J. Kim, G. Kis, P. Klunzinger, Z. Koczor-Benda, J. H. Koh, D. Kosenkov, L. Koulias, T. Kowalczyk, C. M. Krauter, K. Kue, A. Kunitsa, T. Kus, I. Ladjánszki, A. Landau, K. V. Lawler, D. Lefrancois, S. Lehtola, R. R. Li, Y.-P. Li, J. Liang, M. Liebenthal, H.-H. Lin, Y.-S. Lin, F. Liu, K.-Y. Liu, M. Loipersberger, A. Luenser, A. Manjanath, P. Manohar, E. Mansoor, S. F. Manzer, S.-P. Mao, A. V. Marenich, T. Markovich, S. Mason, S. A. Maurer, P. F. McLaughlin, M. F. S. J. Menger, J.-M. Mewes, S. A. Mewes, P. Morgante, J. W. Mullinax, K. J. Oosterbaan, G. Paran, A. C. Paul, S. K. Paul, F. Pavošević, Z. Pei, S. Prager, E. I. Proynov, A. Rák, E. Ramos-Cordoba, B. Rana, A. E. Rask, A. Rettig, R. M. Richard, F. Rob, E. Rossomme, T. Scheele, M. Scheurer, M. Schneider, N. Sergueev, S. M. Sharada, W. Skomorowski, D. W. Small, C. J. Stein, Y.-C. Su, E. J. Sundstrom, Z. Tao, J. Thirman, G. J. Tornai, T. Tsuchimochi, N. M. Tubman, S. P. Veccham, O. Vydrov, J. Wenzel, J. Witte, A. Yamada, K. Yao, S. Yeganeh, S. R. Yost, A. Zech, I. Y. Zhang, X. Zhang, Y. Zhang, D. Zuev, A. Aspuru-Guzik, A. T. Bell, N. A. Besley, K. B. Bravaya, B. R. Brooks, D. Casanova, J.-D. Chai, S. Coriani, C. J. Cramer, G. Cserey, A. E. DePrince III, R. A. DiStasio Jr., A. Dreuw, B. D. Dunietz, T. R. Furlani, W. A. Goddard III, S. Hammes-Schiffer, T. Head-Gordon, W. J. Hehre, C.-P. Hsu, T.-C. Jagau, Y. Jung, A. Klamt, J. Kong, D. S. Lambrecht, W. Liang, N. J. Mayhall, C. W. McCurdy, J. B. Neaton, C. Ochsenfeld, J. A. Parkhill, R. Peverati, V. A. Rassolov, Y. Shao, L. V. Slipchenko, T. Stauch, R. P. Steele, J. E. Subotnik, A. J. W. Thom, A. Tkatchenko, D. G. Truhlar, T. Van Voorhis, T. A. Wesolowski, K. B. Whaley, H. L. Woodcock III, P. M. Zimmerman, S. Faraji, P. M. W. Gill, M. Head-Gordon, J. M. Herbert, and A. I. Krylov, "Software for the frontiers of quantum chemistry: An overview of developments in the Q-Chem 5 package", *J. Chem. Phys.*, **155**, 084801 (2021).

[9] D. R. Nascimento and N. Govind, "Computational approaches for XANES, VtC-XES, and RIXS using linear-response time-dependent density functional theory based methods", *Phys. Chem. Chem. Phys.*, **24**, 14680–14691 (2022).

[10] T. Popmintchev, M.-C. Chen, D. Popmintchev, P. Arpin, S. Brown, S. Ališauskas, G. Andriukaitis, T. Balčiunas, O. D. Mücke, A. Pugzlys, A. Baltuška, B. Shim, S. E. Schrauth, A. Gaeta, C. Hernández-García, L. Plaja, A. Becker, A. Jaron-Becker, M. M. Murnane, and H. C. Kapteyn, "Bright coherent ultrahigh harmonics in the keV x-ray regime from mid-infrared femtosecond lasers", *Science*, **336**, 1287–1291 (2012).

[11] L. Miaja-Avila, G. C. O'Neil, J. Uhlig, C. L. Cromer, M. L. Dowell, R. Jimenez, A. S. Hoover, K. L. Silverman, and J. N. Ullom, "Laser plasma x-ray source for ultrafast time-resolved x-ray absorption spectroscopy", *Struct. Dynam.*, **2**, 024301 (2015).

[12] R. Schoenlein, T. Elsaesser, K. Holldack, Z. Huang, H. Kapteyn, M. Murnane, and M. Woerner, "Recent ad-

vances in ultrafast x-ray sources", *Phil. Trans. R. Soc. A*, **377**, 20180384 (2019).

[13] R. Geneaux, H. J. B. Marroux, A. Guggenmos, D. M. Neumark, and S. R. Leone, "Transient absorption spectroscopy using high harmonic generation: A review of ultrafast x-ray dynamics in molecules and solids", *Phil. Trans. R. Soc. A*, **377**, 20170463 (2019).

[14] A. Depresseux, E. Oliva, J. Gautier, F. Tissandier, J. Nejdl, M. Kozlova, G. Maynard, J. P. Goddet, A. Tafzi, A. Lifschitz, H. T. Kim, S. Jacquemot, V. Malka, K. T. Phuoc, C. Thaury, P. Rousseau, G. Iaquaniello, T. Lefrou, A. Flacco, B. Vodungbo, G. Lambert, A. Rousse, P. Zeitoun, and S. Sebban, "Table-top femtosecond x-ray laser by collisional ionization gating", *Nat. Photonics*, **9**, 817–822 (2015).

[15] J. W. Smith and R. J. Saykally, "Soft x-ray absorption spectroscopy of liquids and solutions", *Chem. Rev.*, **117**, 13909–13934 (2017).

[16] C. Kleine, M. Ekimova, G. Goldsztejn, S. Raabe, C. Strüber, J. Ludwig, S. Yarlagadda, S. Eisebitt, M. J. J. Vrakking, T. Elsaesser, E. T. J. Nibbering, and A. Rouzée, "Soft x-ray absorption spectroscopy of aqueous solutions using a table-top femtosecond soft x-ray source", *J. Phys. Chem. Lett.*, **10**, 52–58 (2019).

[17] T. Suzuki, "Ultrafast photoelectron spectroscopy of aqueous solutions", *J. Chem. Phys.*, **151**, 090901 (2019).

[18] A. D. Smith, T. Balčiūnas, Y.-P. Chang, C. Schmidt, K. Zinchenko, F. B. Nunes, E. Rossi, V. Svoboda, Z. Yin, J.-P. Wolf, and H. J. Wörner, "Femtosecond soft-x-ray absorption spectroscopy of liquids with a water-window high-harmonic source", *J. Phys. Chem. Lett.*, **11**, 1981–1988 (2020).

[19] A. Cirri, J. Husek, S. Biswas, and L. R. Baker, "Achieving surface sensitivity in ultrafast XUV spectroscopy: $M_{2,3}$-edge reflection–absorption of transition metal oxides", *J. Phys. Chem. C*, **121**, 15861–15869 (2017).

[20] J. M. Herbert, "Density-functional theory for electronic excited states", in *Theoretical and Computational Photochemistry: Fundamentals, Methods, Applications and Synergy with Experimental Approaches*, C. García-Iriepa and M. Marazzi, Eds.; Elsevier, 2023; chapter 3, pages 69–118.

[21] M. E. Casida, "Time-dependent density functional response theory for molecules", in *Recent Advances in Density Functional Methods, Part I*, D. P. Chong, Ed., Vol. I of *Recent Advances in Computational Chemistry;* World Scientific: River Edge, NJ, 1995; chapter 5, pages 155–192.

[22] M. E. Casida, "Time-dependent density functional response theory of molecular systems: Theory, computational methods, and functionals", in *Recent Developments and Applications of Modern Density Functional Theory*, J. M. Seminario, Ed., Vol. 4 of *Theoretical and Computational Chemistry;* Elsevier: Amsterdam, 1996; pages 391–439.

[23] F. Furche, "On the density matrix based approach to time-dependent density functional response theory", *J. Chem. Phys.*, **114**, 5982–5992 (2001).

[24] F. Furche and K. Burke, "Time-dependent density functional theory in quantum chemistry", *Annu. Rep. Comput. Chem.*, **1**, 19–30 (2005).

[25] P. Elliott, F. Furche, and K. Burke, "Excited states from time-dependent density functional theory", in *Reviews in Computational Chemistry*, K. B. Lipkowitz and T. R. Cundari, Eds., Vol. 26; Wiley-VCH: New York, 2009; chapter 3, pages 91–165.

[26] M. Stener, G. Fronzoni, and M. de Simone, "Time dependent density functional theory of core electrons excitations", *Chem. Phys. Lett.*, **373**, 115–123 (2003).

[27] D. Zuev, E. Vecharynski, C. Yang, N. Orms, and A. I. Krylov, "New algorithms for iterative matrix-free eigensolvers in quantum chemistry", *J. Comput. Chem.*, **36**, 273–284 (2015).

[28] J. M. Kasper, D. B. Williams-Young, E. Vecharynski, C. Yang, and X. Li, "A well-tempered hybrid method for solving challenging time-dependent density functional theory (TDDFT) systems", *J. Chem. Theory Comput.*, **14**, 2034–2041 (2018).

[29] B. Helmich-Paris, "Simulating X-ray absorption spectra with complete active space self-consistent field linear response methods", *Int. J. Quantum Chem.*, **121**, e26559 (2021).

[30] L. S. Cederbaum, W. Domcke, and J. Schirmer, "Many-body theory of core holes", *Phys. Rev. A*, **22**, 206–222 (1980).

[31] A. Barth and L. S. Cederbaum, "Many-body theory of core-valence excitations", *Phys. Rev. A*, **23**, 1038–1061 (1981).

[32] S. Coriani and H. Koch, "Communication: X-ray absorption spectra and core-ionization potentials within a core-valence separated coupled cluster framework", *J. Chem. Phys.*, **143**, 181103 (2015).

[33] J. Wenzel, A. Holzer, M. Wormit, and A. Dreuw, "Analysis and comparison of CVS-ADC approaches up to third order for the calculation of core-excited states", *J. Chem. Phys.*, **142**, 214104 (2015).

[34] M. L. Vidal, X. Feng, E. Epifanovsky, A. I. Krylov, and S. Coriani, "New and efficient equation-of-motion coupled-cluster framework for core-excited and core-ionized states", *J. Chem. Theory Comput.*, **15**, 3117–3133 (2019).

[35] A. Bussy and J. Hutter, "Efficient and low-scaling linear-response time-dependent density functional theory implementation for core-level spectroscopy of large and periodic systems", *Phys. Chem. Chem. Phys.*, **23**, 4736–4746 (2021).

[36] M. F. Herbst and T. Fransson, "Quantifying the error of the core–valence separation approximation", *J. Chem. Phys.*, **153**, 054114 (2020).

[37] E. K. U. Gross and W. Kohn, "Time-dependent density functional theory", *Adv. Quantum Chem.*, **21**, 255–291 (1990).

[38] E. K. U. Gross, C. A. Ullrich, and U. J. Gossmann, "Density functional theory of time-dependent systems", in *Density Functional Theory*, E. K. U. Gross and R. M. Dreizler, Eds.; Plenum Press: New York, 1995; pages 149–171.

[39] E. K. U. Gross and N. T. Maitra, "Introduction to TDDFT", in *Fundamentals of Time-Dependent Density Functional Theory*, M. A. L. Marques, N. T. Maitra, F. M. S. Nogueira, E. K. U. Gross, and A. Rubio, Eds., Vol. 837 of *Lecture Notes in Physics;* Springer-Verlag: Heidelberg, 2012; chapter 1, pages 53–97.

[40] C. A. Ullrich and Z. H. Yang, "A brief compendium of time-dependent density functional theory", *Braz. J. Phys.*, **44**, 154–188 (2014).

[41] R. Baer and L. Kronik, "Time-dependent generalized Kohn–Sham theory", *Eur. Phys. J. B*, **91**, 170 (2018).

[42] M. R. Provorse and C. M. Isborn, "Electron dynamics with real-time time-dependent density functional theory", *Int. J. Quantum Chem.*, **116**, 739–749 (2016).

[43] X. Li, N. Govind, C. Isborn, A. E. DePrince III, and K. Lopata, "Real-time time-dependent electronic structure theory", *Chem. Rev.*, **120**, 9951–9993 (2020).

[44] S. Tussupbayev, N. Govind, K. Lopata, and C. J. Cramer, "Comparison of real-time and linear-response time-dependent density functional theories for molecular chromophores ranging from sparse to high densities of states", *J. Chem. Theory Comput.*, **11**, 1102–1109 (2015).

[45] Y. Zhu and J. M. Herbert, "Self-consistent predictor/corrector algorithms for stable and efficient integration of the time-dependent Kohn-Sham equation", *J. Chem. Phys.*, **148**, 044117 (2018).

[46] M. Yang, A. Sissay, M. Chen, and K. Lopata, "Intruder peak-free transient inner-shell spectra using real-time simulations", *J. Chem. Theory Comput.*, **18**, 992–1002 (2022).

[47] A. Castro, M. A. L. Marques, and A. Rubio, "Propagators for the time-dependent Kohn–Sham equations", *J. Chem. Phys.*, **121**, 3425–3433 (2004).

[48] X. Li, S. M. Smith, A. N. Markevitch, D. A. Romanov, R. J. Levis, and H. B. Schlegel, "A time-dependent Hartree–Fock approach for studying the electronic optical response of molecules in intense fields", *Phys. Chem. Chem. Phys.*, **7**, 233–239 (2005).

[49] D. Williams-Young, J. J. Goings, and X. Li, "Accelerating real-time time-dependent density functional theory with a nonrecursive Chebyshev expansion of the quantum propagator", *J. Chem. Theory Comput.*, **12**, 5333–5338 (2016).

[50] S. Blanes, F. Casas, and A. Murua, "Symplectic time-average propagators for the Schrödinger equation with a time-dependent Hamiltonian", *J. Chem. Phys.*, **146**, 114109 (2017).

[51] A. G. Pueyo, M. A. L. Marques, A. Rubio, and A. Castro, "Propagators for the time-dependent Kohn–Sham equations: Multistep, Runge–Kutta, exponential Runge–Kutta, and commutator free Magnus method", *J. Chem. Theory Comput.*, **14**, 3040–3052 (2018).

[52] L. Ye, H. Wang, Y. Zhang, and W. Liu, "Self-adaptive real-time time-dependent density functional theory for core excitations", *J. Chem. Phys.*, **157**, 074106 (2022).

[53] A. V. Oppenheim, *Discrete-Time Signal Processing*, Pearson Education: Upper Saddle River, New Jersey, 3rd ed., 1999.

[54] E. Coccia, B. Mussard, M. Labeye, J. Caillat, R. Taïeb, J. Toulouse, and E. Luppi, "Gaussian continuum basis functions for calculating high-harmonic generation spectra", *Int. J. Quantum Chem.*, **116**, 1120–1131 (2016).

[55] Y. Zhu and J. M. Herbert, "High harmonic spectra computed using time-dependent Kohn-Sham theory with Gaussian orbitals and a complex absorbing potential", *J. Chem. Phys.*, **156**, 204123 (2022).

[56] K. Lopata and N. Govind, "Modeling fast electron dynamics with real-time time-dependent density functional theory: Application to small molecules and chromophores", *J. Chem. Theory Comput.*, **7**, 1344–1355 (2011).

[57] K. Lopata, B. E. Van Kuiken, M. Khalil, and N. Govind, "Linear-response and real-time time-dependent density functional theory studies of core-level near-edge x-ray absorption", *J. Chem. Theory Comput.*, **8**, 3284–3292 (2012).

[58] K. Lopata and N. Govind, "Near and above ionization electronic excitations with non-Hermitian real-time time-dependent density functional theory", *J. Chem. Theory Comput.*, **9**, 4939–4946 (2013).

[59] R. G. Fernando, M. C. Balhoff, and K. Lopata, "X-ray absorption in insulators with non-Hermitian real-time time-dependent density functional theory", *J. Chem. Theory Comput.*, **11**, 646–654 (2015).

[60] J. J. Goings and X. Li, "An atomic orbital based real-time time-dependent density functional theory for computing electronic circular dichroism band spectra", *J. Chem. Phys.*, **144**, 234102 (2016).

[61] E. S. S. Hansen, S. Kim, J. J. Miller, M. Geferath, G. Morrell, and C. Laustsen, "Fase Padé transform accelerated CSI for hyperpolarized MRS", *Tomography*, **2**, 117–124 (2016).

[62] D. Belkić and K. Belkić, "Review of recent applications of the conventional and derivative fast Padé transform for magnetic resonance spectroscopy", *J. Math. Chem.*, **57**, 385–464 (2019).

[63] J. J. Goings, J. M. Kasper, F. Egidi, S. Sun, and X. Li, "Real time propagation of the exact two component time-dependent density functional theory", *J. Chem. Phys.*, **145**, 104107 (2016).

[64] D. R. Nascimento and A. E. DePrince, III, "Simulation of near-edge X-ray absorption fine structure with time-dependent equation-of-motion coupled-cluster theory", *J. Phys. Chem. Lett.*, **8**, 2951–2957 (2017).

[65] A. Bruner, D. LaMaster, and K. Lopata, "Accelerated broadband spectra using transition dipole decomposition and Padé approximants", *J. Chem. Theory Comput.*, **12**, 3741–3750 (2016).

[66] P. J. Lestrange, P. D. Nguyen, and X. Li, "Calibration of energy-specific TDDFT for modeling K-edge XAS spectra of light elements", *J. Chem. Theory Comput.*, **11**, 2994–2999 (2015).

[67] N. A. Besley, "Fast time-dependent density functional theory calculations of the x-ray absorption spectroscopy of large systems", *J. Chem. Theory Comput.*, **12**, 5018–5025 (2016).

[68] M. W. D. Hanson-Heine, M. W. George, and N. A. Besley, "Assessment of time-dependent density functional theory calculations with the restricted space approximation for excited state calculations of large systems", *Mol. Phys.*, **116**, 1452–1459 (2018).

[69] N. A. Besley, M. J. G. Peach, and D. J. Tozer, "Time-dependent density functional theory calculations of near-edge x-ray absorption fine structure with short-range corrected functionals", *Phys. Chem. Chem. Phys.*, **11**, 10350–10358 (2009).

[70] N. A. Besley and F. A. Asmuruf, "Time-dependent density functional theory calculations of the spectroscopy of core electrons", *Phys. Chem. Chem. Phys.*, **12**, 12024–12039 (2010).

[71] M. A. Rohrdanz and J. M. Herbert, "Simultaneous benchmarking of ground- and excited-state properties with long-range-corrected density functional theory", *J. Chem. Phys.*, **129**, 034107 (2008).

[72] R. M. Richard and J. M. Herbert, "Time-dependent density-functional description of the ^1L_a state in polycyclic aromatic hydrocarbons: Charge-transfer character in disguise?", *J. Chem. Theory Comput.*, **7**, 1296–1306 (2011).

[73] P. M. W. Gill, B. G. Johnson, and J. A. Pople, "A standard grid for density-functional calculations", *Chem.*

Phys. Lett., **209**, 506–512 (1993).

[74] S. Jana and J. M. Herbert, "Slater transition methods for core-level electron binding energies", *J. Chem. Phys.*, **158**, 094111 (2023).

[75] S. Jana and J. M. Herbert, "Fractional-electron and transition-potential methods for core-to-valence excitation energies using density functional theory", *J. Chem. Theory Comput.* (in press; DOI: 10.1021/acs.jctc.3c00202).

[76] A. Nakata, Y. Imamura, T. Otsuka, and H. Nakai, "Time-dependent density functional theory calculations for core-excited states: Assessment of standard exchange-correlation functionals and development of a novel hybrid functional", *J. Chem. Phys.*, **124**, 094105 (2006).

[77] A. Nakata, Y. Imamura, and H. Nakai, "Hybrid exchange-correlation functional for core, valence, and Rydberg excitations: Core-valence-Rydberg B3LYP", *J. Chem. Phys.*, **125**, 064109 (2006).

[78] A. Nakata, Y. Imamura, and H. Nakai, "Extension of the core-valence-Rydberg B3LYP functional to core-excited-state calculations of third-row atoms", *J. Chem. Theory Comput.*, **3**, 1295–1305 (2007).

[79] M. Roemelt, M. A. Beckwith, C. Duboc, M.-N. Collomb, F. Neese, and S. DeBeer, "Manganese K-edge x-ray absorption spectroscopy as a probe of metal–ligand interactions in coordination compounds", *Inorg. Chem.*, **51**, 680–687 (2012).

[80] T. Fransson, I. E. Brumboiu, M. L. Vidal, P. Norman, S. Coriani, and A. Dreuw, "XABOOM: An x-ray absorption benchmark of organic molecules based on carbon, nitrogen, and oxygen 1s $\rightarrow \pi^*$ transitions", *J. Chem. Theory Comput.*, **17**, 1618–1637 (2021).

[81] F. A. Asmuruf and N. A. Besley, "Calculation of near-edge x-ray absorption fine structure with the CIS(D) method", *Chem. Phys. Lett.*, **463**, 267–271 (2008).

[82] O. Takahashi, "Relativistic corrections for single- and double-core excitations at the K- and L-edges from Li to Kr", *Comput. Theor. Chem.*, **1102**, 80–86 (2017).

[83] Y. Yao, D. Golze, P. Rinke, V. Blum, and Y. Kanai, "All-electron BSE@*GW* method for *K*-edge core electron excitation energies", *J. Chem. Theory Comput.*, **18**, 1569–1583 (2022).

[84] K. C. Prince, R. Richter, M. de Simone, M. Alagia, and M. Coreno, "Near edge x-ray absorption spectra of some small polyatomic molecules", *J. Phys. Chem. A*, **107**, 1955–1963 (2003).

[85] N. A. Besley, A. T. B. Gilbert, and P. M. W. Gill, "Self-consistent-field calculations of core excited states", *J. Chem. Phys.*, **130**, 124308 (2009).

[86] R. Sarangi, M. L. Vidal, S. Coriani, and A. I. Krylov, "On the basis set selection for calculations of core-level states: Different strategies to balance cost and accuracy", *Mol. Phys.*, **118**, e1769872 (2020).

[87] A. E. A. Fouda and N. A. Besley, "Assessment of basis sets for density functional theory-based calculations of core-electron spectroscopies", *Theor. Chem. Acc.*, **137**, 6 (2018).

[88] M. A. Ambroise and F. Jensen, "Probing basis set requirements for calculating core ionization and core excitation spectroscopy by the Δ self-consistent-field approach", *J. Chem. Theory Comput.*, **15**, 325–337 (2019).

[89] M. A. Ambroise, A. Dreuw, and F. Jensen, "Probing basis set requirements for calculating core ionization and core excitation spectra using correlated wave function methods", *J. Chem. Theory Comput.*, **17**, 2832–2842 (2021).

[90] D. E. Woon and T. H. Dunning Jr., "Gaussian basis sets for use in correlated molecular calculations. V. Core-valence basis sets for boron through neon", *J. Chem. Phys.*, **103**, 4572–4585 (1995).

[91] M. W. D. Hanson-Heine, M. W. George, and N. A. Besley, "Basis sets for the calculation of core-electron binding energies", *Chem. Phys. Lett.*, **699**, 279–285 (2018).

[92] J. M. Herbert, "The quantum chemistry of loosely-bound electrons", in *Reviews in Computational Chemistry*, A. L. Parill and K. Lipkowitz, Eds., Vol. 28; Wiley-VCH: Hoboken, 2015; chapter 8, pages 391–517.

[93] F. de Groot and A. Kotani, *Core Level Spectroscopy of Solids*, CRC Press: Boca Raton, 2008.

[94] E. Gousseva, S. D. Midgley, J. M. Seymour, R. Seidel, R. Grau-Crespo, and K. R. J. Lovelock, "Understanding x-ray photoelectron spectra of ionic liquids: Experiments and simulations of 1-butyl-3-methylimidazolium thiocyanate", *J. Phys. Chem. B*, **126**, 10500–10509 (2022).

[95] R. M. Fogerty, R. P. Matthews, M. T. C. andd C. R. Ashworth, A. Brandt-Talbot, P. J. Corbett, R. G. Palgrave, R. A. B. andd T. W. Chamberlain, T. V. Hoogerstaete, P. B. J. Johnson, P. A. Hunt, N. A. Besley, and K. R. J. Lovelock, "NEXAFS spectroscopy of ionic liquids: Experiments versus calculations", *Phys. Chem. Chem. Phys.*, **19**, 31156–31167 (2017).

[96] J. M. Herbert, "Fantasy versus reality in fragment-based quantum chemistry", *J. Chem. Phys.*, **151**, 170901 (2019).

[97] P. E. Bowling, D. R. Broderick, and J. M. Herbert, "Fragment-based calculations of enzymatic thermochemistry require dielectric boundary conditions", *J. Phys. Chem. Lett.*, **14**, 3826–3834 (2023).

[98] V. Gavini, S. Baroni, V. Blum, D. R. Bowler, A. Buccheri, J. R. Chelikowsky, S. Das, W. Dawson, P. Delugas, M. Dogan, C. Draxl, G. Galli, L. Genovese, P. Giannozzi, M. Giantomassi, X. Gonze, M. Govoni, A. Gulans, F. Gygi, J. M. Herbert, S. Kokott, T. K. Kühne, K.-H. Liou, T. Miyazaki, P. Motamarri, A. Nakata, J. E. Pask, C. Plessl, L. E. Ratcliff, R. M. Richard, M. Rossi, R. Schade, M. Scheffler, O. Schütt, P. Suryanarayana, M. Torrent, L. Truflandier, T. L. Windus, Q. Xu, V. W.-Z. Yu, and D. Perez, "Roadmap on electronic structure codes in the exascale era", *Model. Simul. Mater. Sci. Eng.* (in press; preprint available at DOI: 10.48550/arXiv.2209.12747).

[99] L. Konecny, J. Vicha, S. Komorovsky, K. Ruud, and M. Repisky, "Accurate x-ray absorption spectra near L- and M-edges from relativistic four-component damped response time-dependent density functional theory", *Inorg. Chem.*, **61**, 830–846 (2022).

[100] "Ohio Supercomputer Center", http://osc.edu/ark:/19495/f5s1ph73, accessed 2022-06-18.

Table of Contents Graphic